Sensitivity Analysis of Coupled Flutter Instability of Suspension Bridge with Respect to Deck Parameters

HAFID MATAICH*
Laboratory of Informatics and Interdisciplinary Physics (Lipi)
High Normal School
Sidi Mohamed Ben Abdellah University
30040 Fez
MOROCCO

ORCID : https://orcid.org/0009-0009-9210-5603

**Corresponding Author*

Abstract: - The sensitivity of the flutter of a suspension bridge to the mechanical parameters of its deck is a crucial analysis for ensuring the structural stability and safety of the bridge. Flutter, or aeroelastic instability, is a dynamic phenomenon where aerodynamic forces interact with the natural vibrations of the bridge, potentially leading to an exponential growth of oscillations. In this paper, I will analyze the magnitude of the impact that controlling and modifying the bridge's mechanical and geometrical properties, as well as the flow shape of its surface, can have on the point of emergence of a floating aeroelastic instability in a suspension bridge. Using a multimodal approach to calculate the critical floating velocity of the suspension bridge, a formulation that takes into account the lateral, vertical and torsional motions of the bridge deck structure was employed. On the other hand, parametric studies are carried out to identify the parameters that most affect intermodal coupling and modified aerodynamic damping. The role of each float derivative is also discussed. This easy-to-understand formulation makes it possible to identify the most significant modes for a multi-mode aeroelastic instability of the Moroccan Mohamed VI bridge. For this reason, a nonlinear eigenvalue problem is solved with an iterative numerical algorithm that returns the damping ratio of the bridge structure, as well as the critical wind speed.

Key-Words: - Pont suspendu ; Analyse de sensibilité ; Instabilité de flottement ; Instabilité aéroélastique ; Couplage intermodal ; Couplage flexion–torsion ; Dynamique des structures ; Vibrations aéroélastiques ; Flutter aéroélastique

Received: March 29, 2026. Revised: August 2, 2026. Accepted: August 27, 2026. Available online: November 27, 2026.

1 Introduction

The sensitivity of the flutter of a suspension bridge to the mechanical parameters of its deck is a crucial analysis for ensuring the structural stability and safety of the bridge, as shown in the study by [1]. The aerodynamic flutter of suspension bridges is a complex and potentially dangerous phenomenon that has attracted the attention of civil engineers since the first major cable bridge constructions. [2], [3] have reported that this phenomenon occurs when wind-induced aerodynamic forces interact with the vibration modes of the bridge deck, causing increasing oscillations that can lead to structural instability and even collapse. In this article, I will show that the sensitivity of flutter to mechanical deck parameters is crucial to understanding how variations in these parameters can influence the dynamic stability of the bridge. Key mechanical deck parameters, such as bending stiffness, torsional stiffness, linear mass, structural damping and aerodynamic deck shape, play a key role in determining the bridge's response to wind loads.

Bridge engineering designers are very concerned about wind-induced vibrations in long-span suspension or cable-stayed bridges. The fundamental torsion and vertical bending modes of these bridges are characterized by significantly low vibration frequencies. As a result, long-span bridges become extremely vulnerable to self-excited oscillations resulting from the interaction between wind and bridge structure, which have been shown to cause catastrophic destruction in the past. As presented in the following literature [4], [5], [6], [7]. Previous studies that offer more varied methods and formulations to accurately assess self-excited aeroelastic instabilities such as [8], [9], [10], [11],

[12]. The aerodynamic behavior of cables and suspended decks has been described by analytical and numerical studies illustrated in, [13] and [14]. Using a parametric formulation, [15], have been carried out a study of a three-span suspension bridge which is an entirely new type of construction. An analysis to study the phenomenon of flutter instability in long-span suspension bridges for torsional modes was presented by [16], [17], [18]. There are also studies by the researchers, [19], [20], and [21]; these authors studied the instability of structures modeling a suspension bridge in a nonlinear manner, as well as the nonlinear coupling between vibration modes and the modeling of cable bridge structures subjected to nonlinear aeroelastic self-excited forces. [22] used two types of aerodynamic excitation, namely motion-induced wake vortex excitation and Von Karman vortex excitation, for the aeroelastic instability of rectangular structures modeling the deck of the t suspension bridge.

The Mohammed VI cable-stayed bridge in Morocco (As illustrated in Figure 1) is one of the country's most emblematic infrastructures. Inaugurated in July 2016, this bridge, also known as the UMA (Union du Maghreb Arabe) Bridge, is a feat of modern engineering and a symbol of development for Morocco. Part of the Rabat-Casablanca freeway, the Mohammed VI Bridge crosses the Oued Bouregreg, linking the capital Rabat to the city of Salé (As can be seen in Figure 2).



Fig. 1: Mohammed VI suspension bridge over the Oued Bouregreg, Source [22]
Source: created by the authors.



Fig. 2: Topographical map of the Mohamed VI suspension bridge in Morocco,
Source [23]

In this context, sensitivity analysis involves assessing the impact of variations in the bridge's mechanical, geometric, and aerodynamic parameters on the critical wind speed for aeroelastic flutter. This analysis is essential for designing suspension bridges that not only resist static loads but also complex wind-induced dynamic effects. By exploring how each parameter contributes to bridge stability, engineers can optimize deck design to maximize the safety and durability of these iconic structures.

2 Mathematical Formulation of the Problem Under Study

2.1 Formulation assumptions

In this study, the assumptions and approximations that form the basis of this work are inspired by the framework of [24], [25] and [26] as follows

1. Quasi-stationarity: Wind fluctuations adapt instantaneously to the moving bridge deck.
2. Linearity: Based on Taylor expansion to order 1, we neglect the higher-order terms of the aerodynamic forces. As such, aerodynamic damping is assumed to vary linearly with mean wind speed.

2.2 Equation of coupled modal movements

We assume a bridge deck cross-section. Neglecting static and wind turbulence effects, the self-excited aeroelastic forces, as shown in Figure 3, are separated into three components: drag force D_{ar}lift L_{ar} and the deck pitching moment M_{ar}

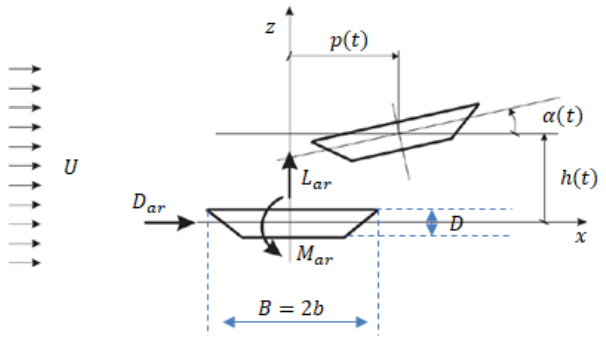

Fig. 3: Deck cross-section, displacements and self-excited aeroelastic forces
Source : Created by the author

For the sake of brevity, the equation of motion for the three degrees of freedom ($p(x,t)$: drag, $h(x,t)$: lift and $\alpha(x,t)$: rotation) can be formed in the form represented by Eq. (1). For those wishing further illustrative steps, they can see the reference [27].

$$[M_s]\{\ddot{Q}(x,t)\} + [C_s]\{\dot{Q}(x,t)\} + [K_s]\{Q(x,t)\} = [C_{ae}]\{\dot{Q}(x,t)\} + [K_{ae}]\{Q(x,t)\} \quad (1)$$

In which the structural matrices of mass, damping and stiffness are, respectively $[M_s], [C_s]\ and\ [K_s]$ and the aerodynamic matrices of self-excited wind-bridge forces are added damping $[C_{ae}]$ and added stiffness $[K_{ae}]$while, $\{Q(x,t)\} = \{p(x,t), h(x,t), \alpha(x,t)\}^T$ represents the three degrees of freedom (3DOF). Consequently, the aeroelastic self-excited forces (lift, drag and moment) are expressed, according to the work of [28], [29], per unit of languor as linear combinations of the 18 float derivatives, $P_i^*, H_i^*, A_i^*\ with\ i = \{1,2 \dots 6\}$ as follows

$$D_{ar}(t) = \frac{\rho U^2(2b)}{2}\left(kP_1^*\frac{\dot{h}}{U} + kP_2^*\frac{b\dot{\alpha}}{U} + k^2P_3^*\alpha + k^2P_4^*\frac{h}{b} + kP_5^*\frac{\dot{p}}{U} + k^2P_6^*\frac{p}{b}\right) \quad (2a)$$

$$L_{ar}(t) = \frac{\rho U^2(2b)}{2}\left(kH_1^*\frac{\dot{h}}{U} + kH_2^*\frac{b\dot{\alpha}}{U} + k^2H_3^*\alpha + k^2H_4^*\frac{h}{b} + kH_5^*\frac{\dot{p}}{U} + k^2H_6^*\frac{p}{b}\right) \quad (2b)$$

$$M_{ar}(t) = \frac{\rho U^2(2b)^2}{2}\left(kA_1^*\frac{\dot{h}}{U} + kA_2^*\frac{b\dot{\alpha}}{U} + k^2A_3^*\alpha + k^2A_4^*\frac{h}{b} + kA_5^*\frac{\dot{p}}{U} + k^2A_6^*\frac{p}{b}\right) \quad (2c)$$

Aerodynamic derivatives, P_i^*, H_i^*, A_i^* are determined taking into account the reduced frequency $k(\omega)$ and depend on the deck geometry (width$B = 2b$) and wind flow (mean speed $\bar{U}$ and density ρ). To find the values of the aerodynamic derivatives, the experimental protocol is sufficiently explained in [30].

$$k(\omega) = \frac{\omega b}{U} \quad (3)$$

The drag force $D_{ar}(t)$ and these components associated with lateral vibration are negligible in most cases, [31]. Consequently, the right-hand term of equation Eq. (1) can be written in matrix form as

$$[C_{ae}]\{\dot{Q}(x,t)\} + [K_{ae}]\{Q(x,t)\} = \frac{\rho U^2 B}{2}\begin{bmatrix} \frac{kH_1^*}{U} & \frac{kH_2^* b}{U} \\ \frac{kA_1^*}{2bU} & \frac{kA_2^*}{2U} \end{bmatrix}\{\dot{Q}(x,t)\} + \frac{\rho U^2 B}{2}\begin{bmatrix} \frac{k^2H_4^*}{b} & k^2H_3^* \\ \frac{k^2A_4^*}{2b^2} & \frac{k^2A_3^*}{2b} \end{bmatrix}\{Q(x,t)\} \quad (4)$$

First of all, to estimate the critical wind speeds that can induce the floating instability of a suspension bridge, a free vibration analysis is required to obtain the natural frequencies $\{\omega\} = \{\omega_1, \omega_2 \dots \omega_n\}$ and free vibration modes $[\Phi] = [\Phi_1, \Phi_2 \dots \Phi_n]$ of the bridge. [32] uses a formulation with quality accuracy to obtain the more realistic natural frequencies and eigenmodes of the bridge deck, can be refined with data from the Mohamed VI bridge to obtain the modal parameters. I have not included this method in my article for the sake of brevity. As a result, the projection of the aeroelastic problem Eq. (1) into the equivalent modal basis is

$$[\Phi]^T[M_s][\Phi]\{\ddot{q}(t)\} + [\Phi]^T[C_s][\Phi]\{\dot{q}(t)\} + [\Phi]^T[K_s][\Phi]\{q(t)\} = [\Phi]^T C_{ae}[\Phi]\{\dot{q}(t)\} + [\Phi]^T K_{ae}[\Phi]\{q(t)\}$$

All deck structure matrices $[M] = [\Phi]^T[M_s]\Phi$, $[C] = [\Phi]^T[C_s][\Phi]$ and $[K] = [\Phi]^T[K_s][\Phi]$ or aerodynamic $[C^{ae}] = [\Phi]^T[C_{ae}][\Phi]$ and $[K^{ae}] = [\Phi]^T[K_{ae}][\Phi]$ are written using generalized modal coordinates $\{q(t)\}$ in the $[\Phi]$ as follows

$$[M_s]\{\ddot{q}(t)\} + [C_s]\{\dot{q}(t)\} + [K_s]\{q(t)\} = \frac{\rho U^2}{2}\left(\frac{b}{U}[C^{ae}]\{\dot{q}(t)\} + [K^{ae}]\{q(t)\}\right) \quad (5)$$

With $[M] = \mathrm{diag}(m_j)$, $[C] = \mathrm{diag}(2m_j\xi_s\omega_j)$ and $[K] = \mathrm{diag}(m_j\omega_j^2)$ represent the mass, damping (Rayleigh shape), and stiffness matrices, respectively, in the modal basis used. The subscript "j" corresponds to the j^{ème} mode (perhaps vertical bending or torsion). The damping and aerodynamic stiffness matrices are $[C^{ae}]$ and $[K^{ae}]$ and are expressed as follows $[C^{ae}] = [\Phi]^T[C_{ae}][\Phi]$ and $[K^{ae}] = [\Phi]^T[K_{ae}][\Phi]$ which are not diagonal and not necessarily symmetric.

Knowing that [I] is an identity matrix of the same dimension as the mass matrix M the system Eq. (5) can be put into a more compact form as follows

$$[I]\{\ddot{q}(t)\} + [M]^{-1}\left([C] - \frac{\rho U b}{2}[C^{ae}]\right)\{\dot{q}(t)\} + [M]^{-1}\left([K] - \frac{\rho U^2}{2}[K^{ae}]\right)\{q(t)\} = 0 \quad (6)$$

We go through some reorganizations in a state space, where the variable becomes $\{Y(t)\} = \begin{Bmatrix} q(t) \\ \dot{q}(t) \end{Bmatrix}$ the system of equations Eq. (6) can be expressed as follows

$$\{\dot{Y}\} = [A]\{Y\} (7)$$

In which $[A] = \begin{bmatrix} 0 & [I] \\ -[M]^{-1}[K_1] & -[M]^{-1}[C_1] \end{bmatrix}$ with $[K_1] = [K] - \frac{\rho U^2}{2}[K^{ae}]$ and $[C_1] = [C] - \frac{\rho U b}{2}[C^{ae}]$. Taking harmonic solutions into account $\{Y(t)\} = \phi_\lambda e^{i\lambda t}$ with $\lambda = \omega^2$ the system Eq. (7) can be written as a complex eigenvalue problem since the matrix A is not symmetric, as follows

$$([A] - \lambda[I])\phi_\lambda e^{i\lambda t} = 0 (8)$$

Solving this complex eigenvalue problem yields modified eigenpulsations, modified vibration mode shapes, and modified damping ratios of the structure interacting with wind at an average wind speed. As these eigenparameters are obtained as a function of self-excited forces, they differ from the natural modes obtained for the structure alone and without loading. On the other hand, the aerodynamic matrices $[K^{ae}]$ and $[C^{ae}]$ are expressed in terms of the unknown reduced frequency $k(\omega) = b\omega/\bar{U}$. Consequently, problem Eq. (8) is non-linear and its solution, at mean wind speed $\bar{U}$ is based on an iterative algorithm as presented in [33].

The analysis of aeroelastic instability in this study requires the examination of the coupling of N vibratory modes. In this case, the system Eq. (8) returns a sequence $(\lambda_j)_{j\in(1,2,\dots N)}$ of complex conjugate eigenvalues, written as follows

$$\lambda_j = \alpha_j \pm i\omega_j, \ for\ j = 1,2,\dots N (9)$$

In which ω_j the imaginary part represents the vibration pulsation $(f_j = \omega_j/2\pi)$ and the damping ratio is expressed by the real part of the eigenvalues $\alpha_j$as follows

$$\xi_j = \frac{-\alpha_j}{\sqrt{\alpha_j^2+\omega_j^2}} (10)$$

Stable operation of a suspension bridge under the influence of wind requires positive damping values. Typically, a real bridge sees its damping increase with wind speed up to a certain speed, after which the damping of a given aeroelastic mode decreases rapidly. When the real part of the eigenvalue cancels (the damping of the corresponding mode also cancels) for a critical wind speed U_{cr} called the critical wind speed that triggers the aeroelastic instability of the bridge, the reader who wants more interpretations can consult the reference [34].

2.3 Bridge sensitivity test

Sensitivity analysis in aeroelasticity involves assessing how small variations in bridge deck mechanics or geometry affect the critical wind speed for flotation. One option is to apply the derivative of the equation that forms problem Eq. (8) with respect to the design variable. Some of the eigenvalues found have a zero real part in the critical condition where the aeroelastic flutter instability begins to manifest itself. The following system results from the critical frequency k_{cr} and the critical wind speed U_{cr} in this condition:

$$[A]Y + \frac{k_{cr}U_{cr}}{B} i[I]Y = 0 (11)$$

The complex equation Eq. (11) is the result of differentiating Eq. (8) with respect to a design variable x ∈ [stiffness, geometry, mass, structural damping, aerodynamics,...] and pre-multiplying on the left by the eigenvector ϕ_λ^T is as follows

$$\phi_\lambda^T \frac{\partial[A]}{\partial x} Y + \phi_\lambda^T \frac{\partial[A]}{\partial U_{cr}} Y \frac{\partial U_{cr}}{\partial x} + \phi_\lambda^T \frac{\partial[A]}{\partial k_{cr}} Y \frac{\partial k_{cr}}{\partial x} + \phi_\lambda^T \frac{i}{B}\left(\frac{\partial k_{cr}}{\partial x} U_{cr} + k\frac{\partial U_{cr}}{\partial x}\right)[I]Y = 0 (12)$$

To simplify, let's say

$$\Theta_{Ax} = \phi_\lambda^T \frac{\partial[A]}{\partial x} Y \quad \Theta_{AU_{cr}} = \phi_\lambda^T \frac{\partial[A]}{\partial U_{cr}} Y \quad \Theta_{Ak_{cr}} = \phi_\lambda^T \frac{\partial[A]}{\partial k_{cr}} Y (13)$$

Equation Eq. (12) becomes

$$\Theta_{Ax} + \frac{\partial U_{cr}}{\partial x}\left(\Theta_{AU_{cr}} + \phi_\lambda^T \frac{ik_{cr}}{B}[I]Y\right) + \frac{\partial k_{cr}}{\partial x}\left(\Theta_{Ak_{cr}} + \phi_\lambda^T \frac{iU_{cr}}{B}[I]Y\right) = 0 (14)$$

Let's ask again

$$\Xi_{U_{cr}} = \Theta_{AU_{cr}} + \phi_\lambda^T \frac{ik_{cr}}{B}[I]Y \quad \Xi_k = \Theta_{Ak_{cr}} + \phi_\lambda^T \frac{iU_{cr}}{B}[I]Y (15)$$

Equation Eq. (14) can be written in a more compact form

$$\frac{\partial U_{cr}}{\partial x}\Xi_{U_{cr}} + \frac{\partial k_{cr}}{\partial x}\Xi_{k_{cr}} = -\Theta_{Ax} (16)$$

Knowing that the numbers $\frac{\partial U_{cr}}{\partial x}$ and $\frac{\partial k_{cr}}{\partial x}$ are real, we multiply equation Eq. (16) by the conjugate $\Xi_{U_{cr}}^*$

$$\frac{\partial U_{cr}}{\partial x}\left|\Xi_{U_{cr}}\right|^2 + \frac{\partial k}{\partial x}\Xi_{U_{cr}}^*\Xi_{k_{cr}} = -\Xi_{U_{cr}}^*\Theta_{Ax} (17)$$

By equating the imaginary components of equation (17), we determine the sensitivity of the critical reduced frequency k_{cr} with respect to the design variable x, as follows

$$\frac{\partial k_{cr}}{\partial x} = \frac{-Img\left(\Xi_{U_{cr}}^*\Theta_{Ax}\right)}{Img\left(\Xi_{U_{cr}}^*\Xi_{k_{cr}}\right)} (18)$$

Similarly, we multiply equation Eq. (16) by the conjugate $\Xi_{k_{cr}}^*$. We determine the sensitivity of the critical speed U_{cr} with respect to the design variable x, as follows

$$\frac{\partial U_{cr}}{\partial x} = \frac{-Img\left(\Xi_k^*\Theta_{Ax}\right)}{Img\left(\Xi_{k_{cr}}^*\Xi_{U_{cr}}\right)} (19)$$

This is done to guide engineers in optimizing the deck design to guarantee a sufficient safety margin against aeroelastic floating of the suspension bridge.

3 Numerical Results and Interpretation

As one of Morocco's most advanced infrastructures, the Mohammed VI suspension bridge has complex mechanical and structural characteristics that guarantee its stability and durability. Table 1 provides an overview of the bridge's main mechanical parameters and properties. These values are assumed to be independent of temperature.

Table 1. Main structural and aerodynamic properties of the Mohamed VI bridge

Structural and material property	**Value**
Length of main span (m)	376.00
Beam mass (kg/m)	5350.0
Mass of main cables (kg/m)	408.00
Mass moment of inertia (kg m^2 /m)	82.430
Deck height (m)	2.2000
Deck width (m)	30.000
Static aerodynamic properties	Value
C_D Drag coefficient	+1.00
C_L Lift coefficient	-0.30
C_M Moment coefficient	+0.01
$dC_D/d\alpha$ 1ère derived from drag coefficient	+0.00
$dC_L/d\alpha$ 1ère derived from the departure coefficient	+4.50
$dC_M/d\alpha$ 1ère derived from moment coeff.	-0.50

Source : [35]

The bridge's static aerodynamic parameters are obtained by simulation using the Ansys CFD simulator. For the sake of brevity, I can't list every stage of the work.

3.1 Modal parameters and floating instability of the Mohamed VI bridge

Before looking at the bridge's dynamic response, a modal analysis is carried out in Ansys to identify the natural frequencies and the modal basis. {Φ}. In Table 2, the first six natural frequencies of the vertical and torsional movements of the Mohamed VI bridge have been determined and compared with those found by closed solutions of [36] adapted for the Mohamed VI bridge. Based on several MATLAB program extracts, a multitude of natural modes have been determined, but they are not implemented below for the sake of brevity. For reasons of communication, we propose to denote vertical modes by V and torsional modes by T, symmetrical natural modes by S and asymmetrical by A.

Table 2. Eigenfrequencies of the old Tacoma Bridge compared to the literature

Mode	**Present**	**[36]**	**Difference**
VA1	0.318	0.312	-1.92
VS1	0.501	0.498	-0.60
VS2	0.791	0.745	-6.17
Mode	Present	Ref.	Difference
TS1	1.441	1.404	-2.63
TA1	1.795	1.744	-2.92
TS2	2.396	2.401	+0.20

Source: Created by the author

The results in Table 2 show a better agreement between the frequencies found by the Ansys simulation and those identified by the work of [30]. The corresponding eigenmodes are illustrated in Figure 4 and Figure 5. From Figure 4 and Figure 5, it appears that it is possible, for example, for the TS1 and VA1 modes to couple. However, the coupling of modes cannot be judged solely on the basis of their spatial homogeneity, but also on the proximity of frequencies. The other modes must also be taken into account, as we observe that the frequency of the torsional mode TS1 (1.441 Hz) is close to the frequency of the vertical mode VS4 (1.08 Hz), and so these two modes are candidates for coupling, indicating the onset of aeroelastic bridge instability.

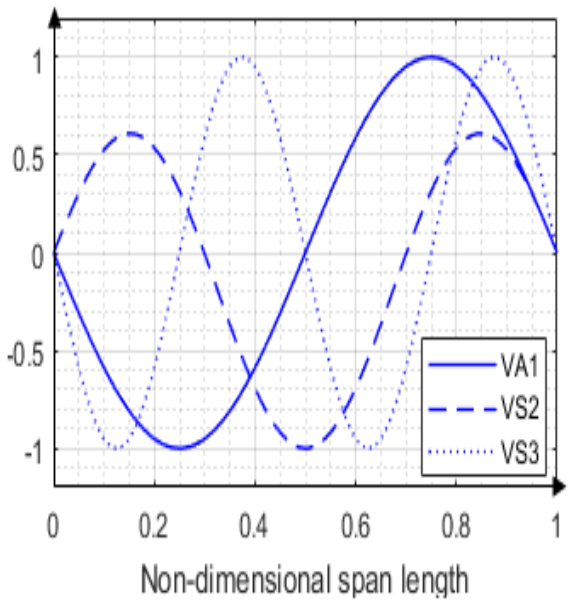

Fig. 4: Transverse modes of free vibration of the Mohamed VI suspension bridge,
Source : Created by the author

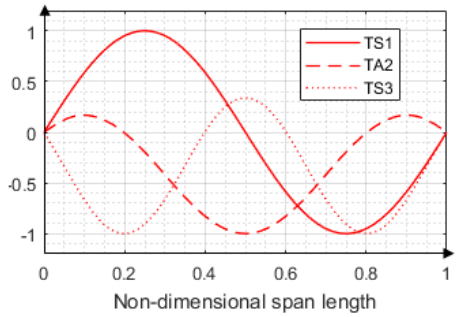

Fig. 5: Free torsional vibration modes of the Mohamed VI suspension bridge,
Source : Created by the author

In Figure 6, the damping corresponding to torsion mode TS1 is the one that crosses the horizontal axis first, indicating that a zero damping value has been reached. As a result, flutter instability will be induced. This figure also shows that the damping of the symmetrical torsional modes TA2 and TS3 tends to decrease above a certain wind speed. On the other hand, there is an increase in damping related to vertical bending modes. In the case of the Mohamed VI suspension bridge, a coupled flutter instability is induced first. The resulting critical wind speed for the bridge's flutter instability is $U_{cr} = 80.1\ m/s$.

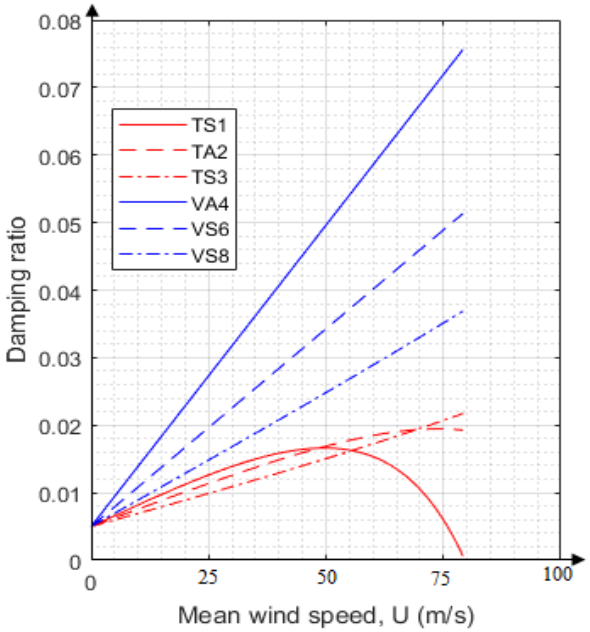

Fig. 6: Mohamed VI suspension bridge modified damping ratio as a function of wind speed,
Source : Created by the author

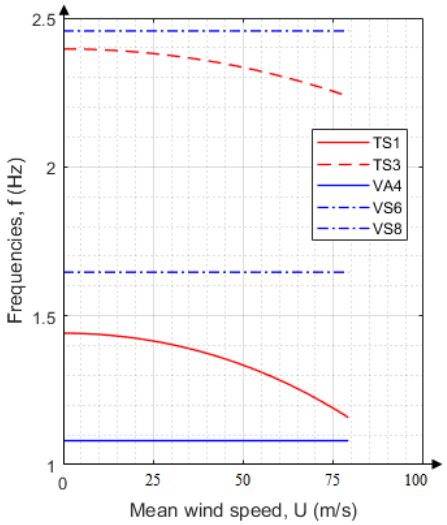

Fig. 7: Evolution of vibration frequencies of the Mohamed VI suspension bridge as a function of wind speed.
Source : Created by the author

Figure 7, on the other hand, mainly shows the evolution of the two frequencies corresponding to the TS1 and VS4 modes. The frequency f_{TS1} tends to decrease with increasing mean wind speed until it crosses that of the VS4 vertical mode, signaling the onset of bridge flutter instability at critical wind speed $U_{cr} = 80.1\ m/s$.

3.2 Mechanical parameters influencing the flotation of the Mohamed VI bridge

3.2.1 Sensitivity to deck bending stiffness ($x = EI$)

In this section, we will discuss the sensitivity of the Mohammed VI bridge's instability to its mechanical stiffness. Figure 8 shows the evolution of the damping ratio of the two modes responsible for the aerodynamic instability of this bridge, the torsional mode TS1 and the vertical mode VS4, after changing the stiffness of the bridge deck from $210.10^9\ N/m^2$ à $450.10^9\ N/m^2$. From the curve characterizing the TS1 torsion mode, it appears that the critical wind speed that allows the bridge to enter unlimited and increasing vibrations increases as the bridge deck becomes stiffer. Figure 9 also confirms that increasing the stiffness of the bridge deck has the effect of raising and increasing natural vibration frequencies significantly.

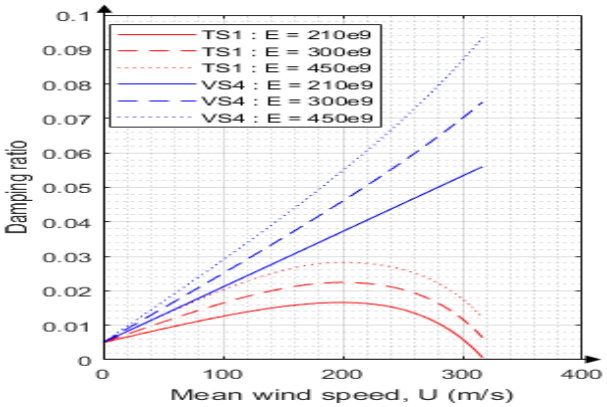

Fig. 8:Sensitivity of float to stiffness on the Mohamed VI suspension bridge,
Source : Created by the author

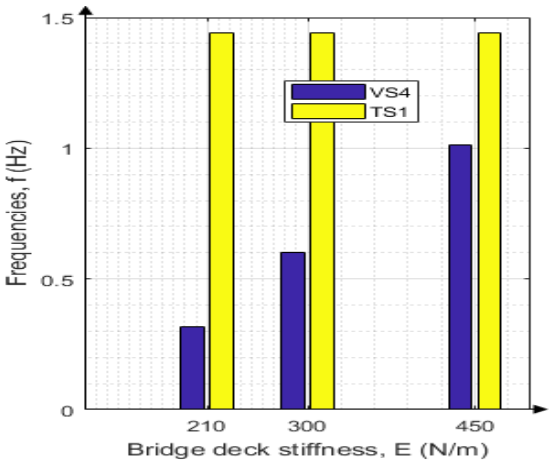

Fig. 9: Sensitivity of natural frequencies to the stiffness of the Mohamed VI suspension bridge,
Source : Created by the author

We conclude that bending stiffness influences the natural frequency of the deck's vertical and torsional vibration modes. An increase in stiffness increases the deck's natural frequencies, making it more resistant to low-frequency flutter. However, higher natural frequencies can also correspond to lower critical flutter speeds, especially if they resonate with aerodynamic excitations. A stiffer structure can dissipate oscillation energy more efficiently, thus improving flutter stability. Torsional rigidity is particularly critical, as flutter is often associated with a coupling between vertical bending and torsional modes. A deck with low torsional stiffness is more likely to develop torsional instabilities at lower wind speeds.

3.2.2 Sensitivity to deck mass ($x = m$)

The sensitivity to deck mass and its distribution also allows us to conclude that the linear mass of the deck directly influences natural frequencies and structural damping. A higher mass tends to reduce natural frequencies, which could lower the critical wind speed for flutter, as shown in Table 3.

Table 3. Sensitivity of the natural frequencies of the Mohamed VI bridge structure and the critical wind speed to the linear distribution of the deck

Deck linear mass in (kg/m)	Natural frequencies in (Hz)		Critical wind speed in (m/s)
	Vertical bending	Twist	
13000	0.318	1.441	80.0
13500	0.285	1.435	78.2

Source: Created by the author

Consequently, an increase in mass increases the inertia of the bridge, reducing the natural frequency and making the system less sensitive to high-frequency oscillations. However, this can lower the critical floating speed. Asymmetrical or irregular mass distribution can lead to a complex dynamic response, potentially increasing sensitivity to flutter.

3.3.3 Sensitivity to structural depreciation ($x = \xi$)

Figure 10 shows the evolution of vertical and torsional natural frequencies when changing the structural damping ratio from 0.005 to 0.01. Figure 11 illustrates the effect of the damping ratio on the critical wind speed for two lengths of the 375 m main span of the Mohamed VI bridge and a fictitious 1200 m span.

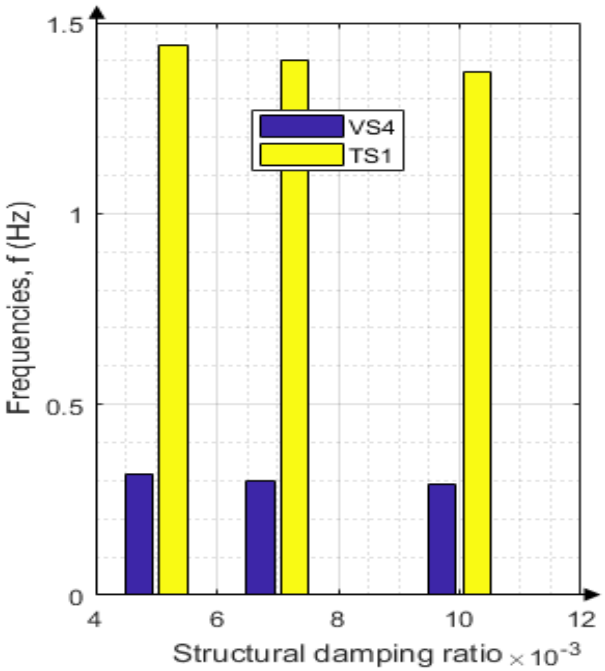

Fig. 10:Sensitivity of natural frequencies to structural damping of Mohamed VI suspension bridge,
Source: Created by the author

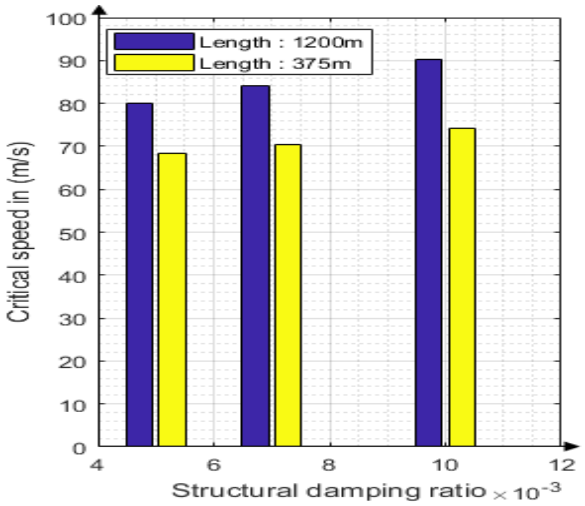

Fig. 11: Sensitivity of critical wind speed to structural damping of Mohamed VI suspension bridge,
Source: Created by the author

According to the two previous figures, damping plays a crucial role in the dissipation of vibratory energy. High damping can significantly increase flutter stability by preventing self-sustained oscillations. Insufficient damping, however, can leave the system vulnerable to flutter, even at relatively low wind speeds. However, the natural structural damping of suspension bridges is often low, sometimes necessitating additional damping devices (dynamic dampers).

3.2.4 Sensitivity to aerodynamic deck shape ($x = C_L, C_M$)

The shape of the deck influences the aerodynamic forces exerted by the wind. An aerodynamic design, with rounded edges or deflectors, can reduce uplift and torsional forces, thus increasing the critical flotation speed. Wind tunnel tests are often necessary to accurately assess the impact of aerodynamic shape on flotation.

We use the Ansys simulator to obtain the aerodynamic coefficients of a modified configuration as shown in Table 4 (Appendix) for Case II. On the basis of the two geometric configurations in Table 4 (Appendix), we find the critical speeds shown in Table 5

Table 5. Sensitivity of critical wind speed to aerodynamic deck shape

Aerodynamic deck shape	Critical wind speed in (m/s)
Case I	80.10
Case II	85.32

Source : Created by the author

Consequently, the coefficients of lift (Cl), drag (Cd), and moment (Cm) define the bridge's response to aerodynamic forces. Variations in these coefficients, due to changes in deck shape or wind angle of attack, can lead to significant changes in dynamic response. Aerodynamic coefficients are not constant and vary with angle of attack, wind speed, and deck shape. Non-linearities can introduce unstable behavior, especially near critical float speeds. Turbulence can induce large-amplitude oscillations, reducing stability. A precise study of the effects of turbulence is needed to determine safety margins.

4 Conclusions

In the literature I have scoured in this field, I have not found a comprehensive study of the aeroelastic instability sensitivity of a bridge, as determined in this study. Consequently, the sensitivity of flotation to mechanical deck parameters is essential for the design and maintenance of suspension bridges, aimed at preventing dynamic instabilities that can lead to catastrophic failures. As a result, the torsional stiffness of the deck directly influences the wind speed at which flotation can be triggered, while mass and damping affect the bridge's ability to dissipate vibratory energy. The floating stability of a suspension bridge is strongly influenced by its mechanical (stiffness, mass, damping) and aerodynamic (aerodynamic coefficients, wind speed, fluid-structure coupling) parameters. The design must therefore optimize these parameters to ensure maximum resistance to flutter. Rigorous analysis using numerical simulations and wind tunnel tests is essential to assess flutter conditions and adapt the design accordingly. The introduction of additional damping systems or optimized aerodynamic shapes can also improve the bridge's resistance to flutter phenomena. For existing bridges, modifications such as adding dampers, reinforcing the deck, or improving the aerodynamic shape may be considered, depending on the sensitivity analysis.

Acknowledgements
The support given to this research project by the Université Sidi Mohamed Ben Abdellah de Fès is gratefully acknowledged. The authors would also like to thank the professors at ENS Fès for their help in correcting the manuscript.

Declaration of Generative AI and AI-assisted Technologies in the Writing Process

During the preparation of this work, the author(s) utilized artificial intelligence (AI) technologies solely for the purpose of linguistic refinement and grammatical correction. Following the application of these tools, the author(s) comprehensively reviewed, verified, and edited the resulting text. The author(s) maintain full accountability and responsibility for the accuracy, integrity, and final content of the publication.

References:

[1] Jurado, J. A., & Hernández, S. (2004). Sensitivity analysis of bridge flutter with respect to mechanical parameters of the deck. Structural and Multidisciplinary Optimization, 27(4), 272–283. https://doi.org/10.1007/s00158-003-0374-8

[2] Chen, X., Matsumoto, M., & Kareem, A. (2000). Aerodynamic coupling effects on flutter and buffeting of bridges. Journal of Engineering Mechanics, 126(1), 17–26. https://doi.org/10.1061/(ASCE)0733-9399(2000)126:1(17)

[3] Cheng, J., Cai, C. S., Xiao, R. C., & Chen, S. R. (2005). Flutter reliability analysis of suspension bridges. Journal of Wind Engineering and Industrial Aerodynamics, 93(10), 757–775. https://doi.org/10.1016/j.jweia.2005.08.003

[4] Arioli, G., & Gazzola, F. (2015). A new mathematical explanation of what triggered the catastrophic torsional mode of the Tacoma Narrows Bridge. Applied Mathematical Modelling, 39(2), 901–912. https://doi.org/10.1016/j.apm.2014.06.022

[5] Abbas, T., Kavrakov, I., & Morgenthal, G. (2017). Methods for flutter stability analysis of long-span bridges : A review. Proceedings of the Institution of Civil Engineers – Bridge Engineering, 170(4), 271–310. https://doi.org/10.1680/jbren.15.00039

[6] Marchionna, C., & Panizzi, S. (2016). An instability result in the theory of suspension bridges. Nonlinear Analysis, 140, 12–28. https://doi.org/10.1016/j.na.2016.03.003

[7] H. Mataich, A. El Amrani and B. El Amrani (2024); Analysis of the thermal instability of laminated composite plates; Coupled Systems Mechanics, Vol. 13, No. 2 pages 95-113; https://doi.org/10.12989/csm.2024.13.2.095

[8] Scanlan, R. H. (1988). On flutter and buffeting mechanisms in long-span bridges. Probabilistic Engineering Mechanics, 3(1), 22–27. https://doi.org/10.1016/0266-8920(88)90004-5

[9] Chen, X., & Kareem, A. (2003). New frontiers in aerodynamic tailoring of long span bridges: An advanced analysis framework. Journal of Wind Engineering and Industrial Aerodynamics, 91(12–15), 1511–1528. https://doi.org/10.1016/j.jweia.2003.09.005

[10] Gianfranco Piana, Alberto Carpinteri (2021); Long-span Suspension Bridge Flutter Analysis with Drag Force Effects; J. Appl. Comput. Mech. 7(SI) 1077-1089; https://doi.org/10.22055/jacm.2021.32481.2025

[11] H. Mataich, A. El Amrani, J. El Mekkaoui and B. El Amrani (2024) ; Effect of flexure-extension coupling on the elastic instability of a composite laminate plate ; Structural Engineering and Mechanics, Vol. 90, No. 4 pages 391-401 ; https://doi.org/10.12989/sem.2024.90.4.391

[12] Wu, T., & Kareem, A. (2013). Bridge aerodynamics and aeroelasticity: A comparison of modeling schemes. Journal of Fluids and Structures, 43, 347–370. https://doi.org/10.1016/j.jfluidstructs.2013.09.015

[13] Arioli, G., & Gazzola, F. (2017). Torsional instability in suspension bridges: The Tacoma Narrows Bridge case. Communications in Nonlinear Science and Numerical Simulation, 42, 342–357. https://doi.org/10.1016/j.cnsns.2016.05.028

[14] Ioannis Raftoyiannis, Theodore Konstantakopoulos and George Michaltsos (2017); Inclined cable-systems in suspended bridges for restricting dynamic deformations; Coupled Systems Mechanics, Vol. 6, No. 4 377-398; https://doi.org/10.12989/csm.2017.6.4.377

[15] Tao, T., Wang, H., & Wu, T. (2018). Parametric study on buffeting performance of a long-span triple-tower suspension bridge. Structure and Infrastructure Engineering, 14(3), 381–399. https://doi.org/10.1080/15732479.2017.1354034

[16] Berchio, E., & Gazzola, F. (2015). A qualitative explanation of the origin of torsional instability in suspension bridges.

Nonlinear Analysis, 121, 54–72. https://doi.org/10.1016/j.na.2014.10.026

[17] Zhang, Z. T., Ge, Y. J., & Yang, Y. X. (2013). Torsional stiffness degradation and aerostatic divergence of suspension bridge decks. Journal of Fluids and Structures, 40, 269–283. https://doi.org/10.1016/j.jfluidstructs.2013.05.001

[18] Zhitian Zhang, Ledong Zhu (2021); Wind-induced symmetric and asymmetric static torsional divergence of flexible suspension bridges; Journal of Fluids and Structures 103 - 103263; https://doi.org/10.1016/j.jfluidstructs.2021.103263

[19] Berchio, E., Ferrero, A., & Gazzola, F. (2016). Structural instability of nonlinear plates modelling suspension bridges : Mathematical answers to some long-standing questions. Nonlinear Analysis: Real World Applications, 28, 91–125. https://doi.org/10.1016/j.nonrwa.2015.09.005

[20] Gao, G., Zhu, L., Li, J., Han, W., & Yao, B. (2020). A novel two-degree-of-freedom model of nonlinear self-excited force for coupled flutter instability of bridge decks. Journal of Sound and Vibration, 480, 115406. https://doi.org/10.1016/j.jsv.2020.115406

[21] Maheux, S., King, J. P. C., El Damatty, A., & Brancaleoni, F. (2020). Assessment of nonlinear structural vertical-torsional coupling in cable-supported bridges. Engineering Structures, 219, 110800. https://doi.org/10.1016/j.engstruct.2020.110800

[22] Mohammed VI Bridge; visited on 07/06/2026, https://en.wikipedia.org/wiki/Mohammed_VI_Bridge

[23] Location of the Mohammed VI Cable-Stayed Bridge ; visited on 07/06/2026 ; https://www.google.com/maps

[24] Matsumoto, M., Yagi, T., Tamaki, H., & Tsubota, T. (2008). Vortex-induced vibration and its effect on torsional flutter instability in the case of B/D = 4 rectangular cylinder. Journal of Wind Engineering and Industrial Aerodynamics, 96(6–7), 971–983. https://doi.org/10.1016/j.jweia.2007.06.023

[25] Mataich Hafid (2025) ; Parametric dynamic instability of a suspension bridge deck under dynamic loading along two of its opposite edges ; Coupled Systems Mechanics, Vol. 14, No. 3, pages 269-288. https://doi.org/10.12989/csm.2025.14.3.269

[26] Li Y., Chen Z., Dong S.-J. and Li, J.-W. (2021); Study on the Effects of Pedestrians on the Aerostatic Response of a Long-Span Pedestrian Suspension Bridge; KSCE Journal of Civil Engineering, 25(10), 3866-3878; https://doi.org/10.1007/s12205-021-2127-x

[27] Salenko, S., Obukhovskiy, A., Gosteev, Y., Yashnov, A., & Lebedev, A. (2021). Strength, flexural rigidity and aerodynamic stability of fiberglass spans in pedestrian suspension bridge. Transportation Research Procedia, 54, 758–767. https://doi.org/10.1016/j.trpro.2021.02.131

[28] Scanlan, R. H. (1996). Aerodynamics of cable-supported bridges. Journal of Constructional Steel Research, 39(1), 51–68. https://doi.org/10.1016/0143-974X(96)00029-6

[29] Scanlan, R. H. (2000). Motion-related body-force functions in two-dimensional low-speed flow. Journal of Fluids and Structures, 14(1), 49–63. https://doi.org/10.1006/jfls.1999.0252

[30] Zhang, X.-J., Ying, F.-B., Zhao, C.-Y., & Pan, X.-R. (2023). Flutter stability of a long-span suspension bridge during erection under skew wind. Wind and Structures, 37(1), 39–56. https://doi.org/10.12989/was.2023.37.1.039

[31] Sebastiano Russo, Gianfranco Piana , Luca Patruno and Alberto Carpinteri (2023) ; Preliminary Flutter Stability Assessment of the Double-Deck George Washington Bridge ; Appl. Sci., 13, 6389. https://doi.org/10.3390/app13116389

[32] Strømmen, E. N. (2014). Structural Dynamics. Springer International Publishing, Cham, XVIII, 510 pp. ISBN 978-3-319-01802-7. https://doi.org/10.1007/978-3-319-01802-7

[33] Nieto, F., Hernández, S., Jurado, J. Á., & Mosquera, A. (2011). Analytical approach to sensitivity analysis of flutter speed in bridges considering variable deck mass. Advances in Engineering Software, 42(4), 117–129. https://doi.org/10.1016/j.advengsoft.2010.12.003

[34] Heremans, J., Mayou, A., & Denoël, V. (2021). Background/Resonant decomposition of the stochastic torsional flutter response of an aeroelastic oscillator under buffeting loads. Journal of Wind Engineering and Industrial Aerodynamics, 208, 104423. https://doi.org/10.1016/j.jweia.2020.104423

[35] Mohammed VI Cable Stayed bridge ; visited on 12/06/2026 ; https://www.adm.co.ma/fr/ouvrages-d-art/pont-a-haubans-mohammed-vi

[36] Strømmen, E. N. (2024). Structural Dynamics (2nd ed.). Springer, Cham. https://doi.org/10.1007/978-3-031-54211-4

[37] Environmental safeguards shape construction of Morocco's longest bridge; visited on 12/06/2026 ; https://en.le360.ma/economy/environmental-safeguards-shape-construction-of-moroccos-longest-bridge-in-laayoune_BXAR3EI3GRGLDOQZPA5QZDETK4/

Contribution of Individual Authors to the Creation of a Scientific Article (Ghostwriting Policy)

All the work presented in this article, including the problem analysis, manuscript writing, simulations, and interpretation of the results, was carried out entirely by me, H. MATAICH.

Sources of Funding for Research Presented in a Scientific Article or Scientific Article Itself

The support given to this research project by the Université Sidi Mohamed Ben Abdellah de Fès is gratefully acknowledged. The authors would also like to thank the professors at ENS Fès for their help in correcting the manuscript.

Conflict of Interest

The author has no conflicts of interest to declare that are relevant to the content of this article.

Creative Commons Attribution License 4.0 (Attribution 4.0 International, CC BY 4.0)

This article is published under the terms of the Creative Commons Attribution License 4.0 https://creativecommons.org/licenses/by/4.0/deed.en_US

APPENDIX

Table 4. Static aerodynamic coefficients of the Mohamed VI bridge

Cross-section of the Mohamed VI bridge		Results obtained from Ansys simulations				
		C_L	$dC_L/d\alpha$	C_M	$dC_M/d\alpha$	C_D
Case I : Original configuration	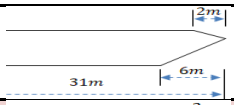	-0.30	+4.50	+0.01	-0.50	+1.00
Case II : Modified configuration	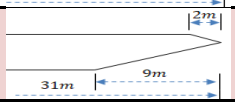	+2.30	+5.50	+0.01	-0.50	+1.01

Source [37]